

Organometallic nickel(II) complexes with substituted benzonitrile ligands. Synthesis, electrochemical studies and non-linear optical properties. The X-ray crystal structure of $[\text{Ni}(\eta^5\text{-C}_5\text{H}_5)\{\text{P}(\text{C}_6\text{H}_5)_3\}(\text{NCC}_6\text{H}_4\text{NH}_2)]\text{[PF}_6\text{]}$

Alberto R. Dias ^a, M. Helena Garcia ^{a,b,*}, Paulo Mendes ^{a,b}, M. Fátima M. Piedade ^{a,b},
M. Teresa Duarte ^a, Maria J. Calhorda ^{b,c}, Carlo Mealli ^d, W. Wenseleers ^e,
A.W. Gerbrandij ^e, Etienne Goovaerts ^e

^a Centro de Química Estrutural, Instituto Superior Técnico, Av. Rovisco Pais, 1096 Lisboa Codex, Portugal

^b Faculdade de Ciências, R. Ernesto de Vasconcelos, Ed. C1, 1700 Lisboa, Portugal

^c ITQB, Apart. 127, 2780 Oeiras, Portugal

^d Istituto per lo Studio della Stereochimica ed Energetica dei Composti di Coordinazione, Via Nardi 39, 50132 Florence, Italy

^e Physics Department, University of Antwerp, Antwerp, Belgium

Received 5 May 1997; received in revised form 13 August 1997

Abstract

A new family of organometallic Ni(II) benzonitrile derivatives bearing strong donor substituents of general formula $[\text{Ni}(\eta^5\text{-C}_5\text{H}_5)\{\text{P}(\text{C}_6\text{H}_5)_3\}\text{NCC}_6\text{H}_4\text{R}]\text{[PF}_6\text{]}$ (R = NH₂, N(CH₃)₂, C₆H₅, OCH₃, H, F) has been synthesized. A structural study by X-ray diffraction of the compound with R = NH₂ showed crystallization on the centrosymmetric monoclinic space group, $P2_1/n$, with a quasi planar structure of the coordinated nitrile. First and second hyperpolarizabilities evaluated by hyper-Rayleigh scattering and Maker fringe techniques showed essentially the same values for the complexes and the uncoordinated chromophores. Theoretical studies by the extended Hückel method found a small amount of π delocalization due to the cancelling effects on the interaction of the metal fragment orbitals with π and π^* nitrile orbitals. © 1998 Elsevier Science S.A.

Keywords: Organometallic Ni; Delocalization; Nitrile orbitals

1. Introduction

In the field of organometallic chemistry, much interest is currently devoted to the synthesis of new materials possessing large second-order nonlinearities, especially because of their potential use in the area of integrated optics [1]. In particular, after the 1987 report of Green et al. [2] on the second harmonic generation efficiency of *cis*-[1-ferrocenyl-2-(4-nitrophenyl)ethylene] the related research [3–8] in this area has increased constantly.

Non-linear optical (NLO) properties have been associated, in organic and in organometallic materials, with highly polarized π -electronic systems which form under an applied electric field associated with a laser beam. Under this perspective, molecules possessing conjugated donor-acceptor systems, are seen as potentially good candidates for the manifestation of the properties. Recently, we published some results on the chemistry and NLO properties, namely SHG efficiencies, of compounds formed by the unit $\text{M}(\eta^5\text{-C}_5\text{H}_5)(\text{P} \cdots \text{P})$ (M = Fe(II), Ru(II)) and *p*-substituted benzonitriles containing ligands [9,10]. Also, we reported on the optical third-harmonic generation (THG) of Ru(II) compounds [11]. This work has been motivated by the reports on the relatively high second harmonic generated signals for some *para*-substituted benzonitriles such as *p*-MeOC₆H₄CN, *p*-H₂NC₆H₄CN [12] and *p*-

* Corresponding author.

MeOC₆H₄C₆H₄CN [13]. We have explored the possibility of enhancing the signals by introducing a NC acceptor group to given organometallic moieties. It is known that normal σ coordination of the NC functional group to a metal center takes place through the nitrogen lone pair. The two sets of orthogonal π and π^* orbitals (more localized on N and C atoms, respectively) may be also involved in interactions with d metal orbitals having the right π symmetry. Therefore, the nitrile group could play an attractive role as its π electron system may be alternatively attracted toward the metal center or toward a π acceptor group located away from the metal. This effect was studied for [Fe(η^5 -C₅H₅)(P \cdots P)]- and [Ru(η^5 -C₅H₅)(P \cdots P)]-fragments (where P \cdots P = bidentate phosphine) attached to the ligand *p*-NCC₆H₄R (R = donor or acceptor substituent). In particular, it was found that, in the case of *p*-NCC₆H₄NO₂, a significant π backdonation from the metal extends through the whole π system and toward the NO₂ acceptor group. The large electron polarization, in some of the systems investigated, reflects in the Kurtz powder and SHG values which were 38 times more efficient than the urea standard in the case of [Fe(η^5 -C₅H₅)(+Diop)(NCC₆H₄NO₂)] [PF₆] [9], and 10 times in the case [Ru(η^5 -C₅H₅)(+Diop)(NCC₆H₄NO₂)] [CF₃SO₃] [10]. The value of the second hyperpolarizability $\gamma(-3\omega; \omega, \omega, \omega)$ of 2.3×10^{-33} esu, measured by maker fringe technique, was found for the ruthenium analogue [Ru(η^5 -C₅H₅)(dppf)(NCC₆H₄C₆H₄NO₂)] [PF₆] [11].

Our continuing studies in this field prompted us to explore the chemistry of other M(η^5 -C₅H₅) based 18 electron complexes and we present here the synthesis and characterization of a new family of nickel(II) derivatives as well as their second and third order NLO properties determined by hyper-Rayleigh scattering and Maker fringe technique, respectively.

2. Results and discussion

2.1. Chemical studies

New nitrile complexes were prepared by chloride abstraction from the parent neutral compound [Ni(η^5 -C₅H₅)(P(C₆H₅)₃)Cl], by TIPF₆ in the presence of a large excess of the NCC₆H₄R adequate nitrile (R = NH₂, N(CH₃)₂, C₆H₅, OCH₃, H, F), in diethyl ether at room temperature. A brown greenish microcrystalline precipitate of [Ni(η^5 -C₅H₅)(P(C₆H₅)₃)NCC₆H₄R]] [PF₆] was obtained with yield in the range of 78–98%, depending on the nitrile, this yield being based on the ¹H NMR spectra of the crude reaction products. The compounds are fairly stable towards oxidation, in air and to moisture, in solid state, but they are not so stable in solution. Special care had to be taken during recrystallization owing to the easy formation of [Ni(η^5 -C₅H₅)(P(C₆H₅)₃)₂]] [PF₆] which was also identified by ¹H NMR as being the major by-product of the studied reaction. Formulation of the new compounds was supported by analytical data, IR and ¹H, ³¹P, ¹³C NMR spectra (Tables 1 and 2) as discussed below. The molar conductivities of

Table 1

¹H NMR data in chloroform-*d* for complexes [NiCpPPh₃(*p*-NCC₆H₄R)] [PF₆]

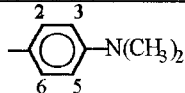
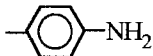
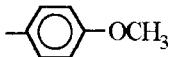
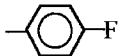
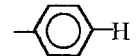
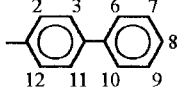
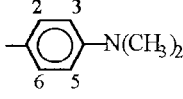
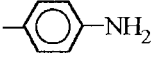
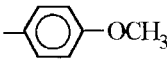
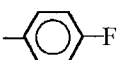
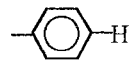
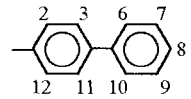
| Compound [NiCpPPh ₃ (<i>p</i> -NCC ₆ H ₄ R)] [PF ₆] | δ (ppm), multiplicity, relative integrals, assignment |
|--|---|
|  | 2.99 (s, 6H, N(CH ₃) ₂); 5.43 (s, 5H, η^5 -C ₅ H ₅); 6.84 (d, 2H, H ₂ ,H ₆); 6.45 (d, 2H, H ₃ ,H ₅) |
|  | 4.53 (b, 2H, NH ₂); 5.42 (s, 5H, η^5 -C ₅ H ₅); 6.46 (d, 2H, H ₃ ,H ₅); 6.73 (d, 2H, H ₂ ,H ₆) |
|  | 3.79 (s, 3H, OCH ₃); 5.46 (s, 5H, η^5 -C ₅ H ₅); 6.78 (d, 2H, H ₃ ,H ₅); 7.04 (d, 2H, H ₂ ,H ₆) |
|  | 5.49 (s, 5H, η^5 -C ₅ H ₅); 7.00 (t, 2H, H ₃ ,H ₅); 7.18 (q, 2H, H ₂ ,H ₆) |
|  | 5.49 (s, 5H, η^5 -C ₅ H ₅); 7.12 (d, 2H, H ₂ ,H ₆); 7.31 (t, 2H, H ₃ ,H ₅); 7.51 (s, 1H, H ₄) |
|  | 5.50 (s, 5H, η^5 -C ₅ H ₅); 7.19 (d, 2H, H ₂ ,H ₁₂); 7.53 (d, 2H, H ₃ ,H ₁₁); 7.42 (s, 2H, H ₇ ,H ₉); 7.50 (s, 2H, H ₆ ,H ₁₀) |

Table 2
 ^{13}C NMR data, in chloroform-*d*, for complexes $[\text{NiCpPPh}_3(p\text{-NCC}_6\text{H}_4\text{R})][\text{PF}_6]$

| Compound $[\text{NiCpPPh}_3(p\text{-NCC}_6\text{H}_4\text{R})][\text{PF}_6]$ | $\delta(\text{ppm})$, assignment |
|---|---|
|  | 39.83 ($\text{N}(\text{CH}_3)_2$); 92.97 (C1); 95.94 ($\eta^5\text{-C}_5\text{H}_5$); 111.26 (C3,C5); 134.14 (C2,C6); 153.44 (C4) |
|  | 95.0 (C1); 95.89 ($\eta^5\text{-C}_5\text{H}_5$); 114.24 (C3,C5); 134.48 (C2,C6); 152.80 (C4) |
|  | 55.75 (OCH_3); 96.22 ($\eta^5\text{-C}_5\text{H}_5$); 100.39 (C1); 114.97 (C3,C5); 135.09 (C2,C6); 164.36 (C4) |
|  | 96.47 ($\eta^5\text{-C}_5\text{H}_5$); 105.58 (C1); 116.96 (C3,C5, $^2J(\text{CF})=24$); 136.01 (C2,C6, $^3J(\text{CF})=10$); 165.98 (C4, $J(\text{CF})=261$) |
|  | 96.44 ($\eta^5\text{-C}_5\text{H}_5$); 109.35 (C1); 129.13 (C3,C5); 132.96 (C2,C6); 134.58 (C4) |
|  | 96.45 ($\eta^5\text{-C}_5\text{H}_5$); 107.70 (C1); 127.23 (C6,C10); 127.60 (C3,C11); 128.97 (C8); 129.10 (C7,C9); 133.46 (C2,C12); 138.57 (C5); 147.25 (C4) |

10^{-3} M solutions of the complexes in nitromethane, in the range $70\text{--}90 \Omega^{-1} \text{ cm}^2 \text{ mol}^{-1}$, were consistent with values reported for 1:1 electrolytes [14].

Typical IR bands confirm the presence of the cyclopentadienyl ligand (3060 cm^{-1}) and the PF_6^- anion (840 and 560 cm^{-1}). A shift of the NC stretching frequency upon coordination is observed in the positive range $20\text{--}45 \text{ cm}^{-1}$. This implies a σ -coordinated nitrile in which the overall $\text{N}\equiv\text{C}$ bond is strengthened upon coordination. At variance with what is found for the previously mentioned for the Fe(II) and Ru(II) analogs, the π back-donation seems non-existent in these Ni(II) complexes.

The ^{13}C NMR data show that amongst the atoms of the nitrile benzene ring only that bound to CN (C_1) is not deshielded. All the others are slightly deshielded as expected when the benzonitrile group is involved in a normal σ coordination. The effects seem to depend on the donor capabilities of the *p*-substituent ($\text{NH}_2 \cong \text{N}(\text{CH}_3)_2 > \text{C}_6\text{H}_5 > \text{OCH}_3 > \text{H} \cong \text{F}$). The highest shielding of the C_1 atom (comparing the free and the coordinated donor nitrile ligands) has a value of 3.9 ppm and it is observed for the $\text{NCC}_6\text{H}_4\text{NH}_2$ substituent. Considering the ^1H NMR data, the protons attached to the carbon atoms are shielded, especially so the *ortho* bonded H_2 , H_6 protons. In particular for the NH_2 case, the shielding was up to 0.69 ppm. A possible explanation can be found by assuming an electronic interaction of the protons with the counter ion, as observed before in our studies of Ru(II) compounds [10]. It was also observed that ^1H and ^{13}C nmr data for $\eta^5\text{-C}_5\text{H}_5$ together with ^{31}P data for PPh_3 ligand were only slightly influenced by the *p*-substituted nitrile group and followed the same general trend of the shielding, presented above. These observations, altogether, suggest some electronic relationship between the *p*-substituted donor group and the metal fragment: in particular, the trends associated with $[\text{Ni}(\eta^5\text{-C}_5\text{H}_5)\{\text{P}(\text{C}_6\text{H}_5)_3\}]^+$ seem to revert the situation previously observed for the Ru(II) and Fe(II) complexes containing the same nitrile ligand. In the latter, the metal essentially behaves as a σ acceptor.

2.2. Crystallographic studies

The crystal structure contains discrete $[\text{Ni}(\eta^5\text{-C}_5\text{H}_5)\text{PPh}_3(\text{NCC}_6\text{H}_4\text{NH}_2)]^+$ cations and $[\text{PF}_6]^-$ anions. A view of the crystal packing, in the centrosymmetric space group $P2_1/n$, is shown in Fig. 1. The complex cation is depicted in Fig. 2 and selected bond lengths and bond angles are listed in Table 3.

The nickel atom is coordinated to one η^5 -cyclopentadienyl ring, one triphenylphosphine, and one $\text{NC}(\text{C}_6\text{H}_4)\text{NH}_2$ ligand. By assuming that Cp occupies three coordination positions, the Ni(II) species can be considered five-coordinated and it obeys the 18 electron rule. The metal atom deviates only $0.062(4) \text{ \AA}$ from the plane formed by the centroid of the Cp ligand and by the donor atoms N(1) and P(1). The coordination angles around the nickel atom, P-Ni-N $95.4(1)^\circ$, P-Ni-Cp $132.9(1)^\circ$, and N-Ni-Cp $131.2(2)^\circ$, are comparable with those in the related $[\text{Ni}(\eta^5\text{-C}_5\text{H}_5)(\text{PPh}_3)(\text{ON}_2\text{C}_6\text{H}_4\text{NO}_2\text{-}p)]$ [17], $96.1(1)^\circ$, 133.8° and 129.2° , respectively.

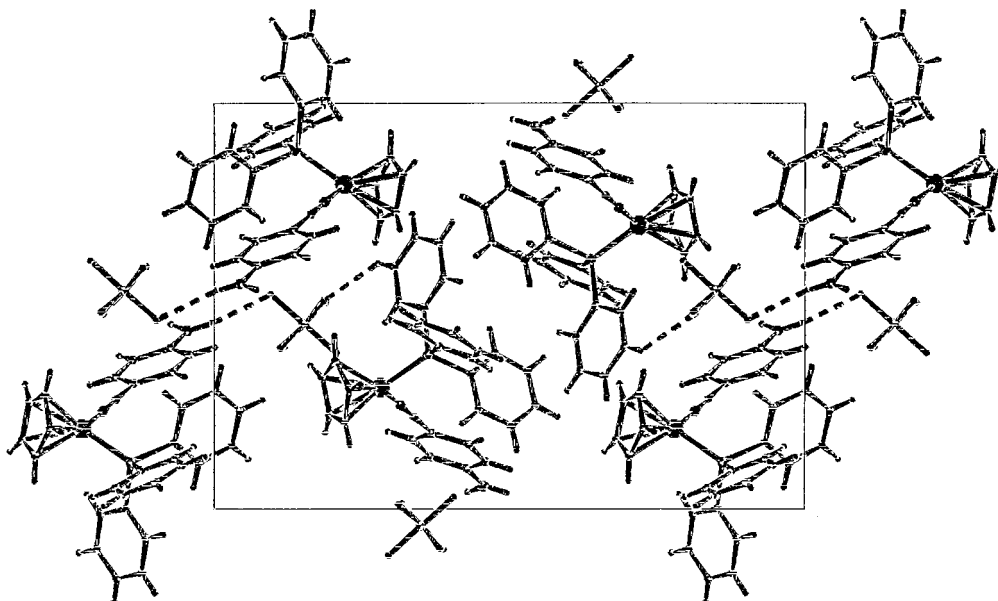


Fig. 1. Molecular diagram showing the crystal packing of $[\text{Ni}(\eta^5\text{-C}_5\text{H}_5)\text{PPh}_3(\text{NCC}_6\text{H}_4\text{NH}_2)]\text{PF}_6$, using SCHAKAL [15].

The Ni–P bond length [2.174(1) Å] is near the upper limit of the range [2.183–2.139 Å] found in the Cambridge Crystallographic Data Base [18] from ten complexes of the type $\text{CpNi}(\text{PPh}_3)\text{L}$. The distance between Ni and the Cp centroid of 1.737(1) Å is similar to that of related triphenylphosphine complexes [1.717–1.763 Å]. The Cp ring is practically planar. The Ni–N bond length in $[\text{Ni}(\eta^5\text{-C}_5\text{H}_5)(\text{PPh}_3)(\text{NCC}_6\text{H}_4\text{NH}_2)]^+$ [1.855(3) Å] is shorter than the ones in other Ni–nitrile complexes, such as $\text{Ni}[(\text{C}_6\text{H}_5)_3\text{P}]_3(\text{NCC}_6\text{H}_5)$, [1.889(11) Å] [19] and $[\text{Ni}(\text{NCC}_6\text{H}_5)\text{P}(\text{C}_6\text{H}_5)_3]_4 \cdot 2\text{C}_7\text{H}_8$, [1.87(2), 1.91(2), 1.89(2), 1.91(3) Å] [20].

The arrangement Ni–N–C–C deviates somewhat from linearity, the angles Ni–N(1)–C(21) and N(1)–C(21)–C(22) being $176.2(4)^\circ$ and $177.5(6)^\circ$, respectively. Also the Ni(1), N(1) and C(21) atoms are out of the plane of the phenyl ring with deviations of 0.366(13), 0.155(10) and 0.074(8) Å, in the order. A non perfectly linear but coplanar geometry has been observed also for the free ligand at room temperature [21]. However, at lower temperature the amino group becomes pyramidal [22].

The N–C distance of 1.124(5) Å appears somewhat shorter than the value 1.15(2) Å, found in the complex $\text{Ni}[(\text{C}_6\text{H}_5)_3\text{P}]_3(\text{NCC}_6\text{H}_5)$ [19] and in the uncoordinated molecule of *p*-aminobenzonitrile [1.143(5) Å]. Nevertheless,

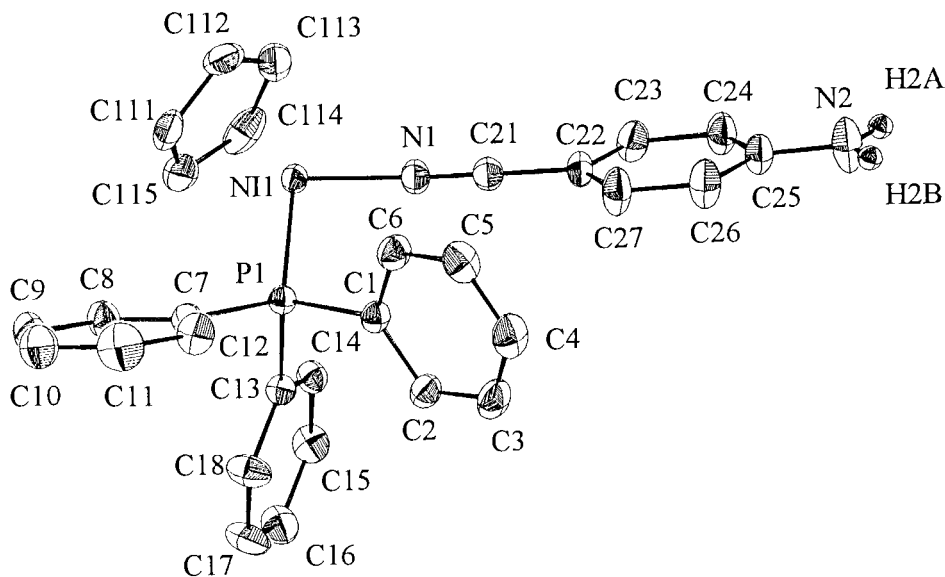


Fig. 2. ORTEP II [16] molecular diagram of the cation $[\text{Ni}(\eta^5\text{-C}_5\text{H}_5)\text{PPh}_3(\text{NCC}_6\text{H}_4\text{NH}_2)]^+$, anisotropic displacement parameters depicted at 50% (?) probability level.

Table 3

Selected bond lengths and bond angles for $[\text{Ni}(\eta^5\text{-C}_5\text{H}_5)\{\text{P}(\text{C}_6\text{H}_5)_3\}(\text{NCC}_6\text{H}_4\text{NH}_2)]\text{[PF}_6\text{]}$

| | | | |
|-------------------------|------------|-------------------|----------|
| <i>Bond lengths (Å)</i> | | | |
| Ni(1)–N(1) | 1.855(3) | Ni(1)–C(111) | 2.064(4) |
| Ni(1)–C(113) | 2.073(5) | Ni(1)–C(115) | 2.091(9) |
| Ni(1)–C(112) | 2.126(5) | Ni(1)–C(114) | 2.133(5) |
| Ni(1)–P(1) | 2.1737(11) | P(1)–C(13) | 1.809(4) |
| P(1)–C(1) | 1.816(4) | P(1)–C(7) | 1.825(4) |
| N(1)–C(21) | 1.124(5) | C(21)–C(22) | 1.422(6) |
| C(22)–C(23) | 1.383(6) | C(22)–C(27) | 1.384(7) |
| C(23)–C(24) | 1.371(6) | C(24)–C(25) | 1.382(7) |
| C(25)–N(2) | 1.362(6) | C(25)–C(26) | 1.392(7) |
| C(26)–C(27) | 1.366(7) | N(2)–H(2A) | 0.92(2) |
| N(2)–H(2B) | 0.894(11) | Ni–Cp | 1.737(1) |
| <i>Bond angles (°)</i> | | | |
| N(1)–Ni(1)–P(1) | 95.4(7) | C(21)–N(1)–Ni(1) | 176.2(4) |
| N(1)–Ni(1)–Cp | 131.2(2) | P(1)–Ni(1)–Cp | 132.9(1) |
| N(1)–C(21)–C(22) | 177.5(6) | C(23)–C(22)–C(27) | 119.1(4) |
| C(23)–C(22)–C(21) | 121.6(4) | C(27)–C(22)–C(21) | 119.3(4) |
| C(24)–C(23)–C(22) | 120.2(4) | C(23)–C(24)–C(25) | 120.9(4) |
| N(2)–C(25)–C(24) | 120.9(5) | N(2)–C(25)–C(26) | 120.4(5) |
| C(24)–C(25)–C(26) | 118.7(4) | C(27)–C(26)–C(25) | 120.3(5) |
| C(26)–C(27)–C(22) | 120.7(5) | C(25)–N(2)–H(2A) | 113(5) |
| C(25)–N(2)–H(2B) | 112(4) | H(2A)–N(2)–H(2B) | 134(6) |

the C–C bond connecting the aromatic ring and the nitrile group, C(21)–C(22), 1.422(6) Å, is shorter than that in the free *p*-aminobenzonitrile [1.430(5) Å] [21] and than the corresponding bond length in $\text{Ni}[(\text{C}_6\text{H}_5)_3\text{P}]_3(\text{NCC}_6\text{H}_5)$ [1.44(2) Å] [19]. The bonds between the *ortho* and *meta* carbons, [C(23)–C(24) 1.371(6) and C(26)–C(27) 1.366(7) Å], are slightly shorter than the other C–C bonds in the phenyl ring, which range from 1.382(7) to 1.392(7) Å. The N(2)–phenyl bond length of 1.362(6) Å in the complex is analogous to that in the free ligand at room temperature, 1.360(5) Å [21] and shorter than the one found in the free ligand at lower temperature, where the amino group is pyramidalized [22].

The crystal structure exhibits short contacts between one hydrogen atom of NH_2 and the PF_6^- anion [H(2B) \cdots F(1) 2.692 and H(2B) \cdots F(2) 2.394 Å, see Fig. 1]. This also causes the two hydrogen atoms to be distinct. Intermolecular interactions between the hydrogens of one phenyl ring of the triphenylphosphine and fluorines of the PF_6^- anion are also observed [H(15) \cdots F(4) 2.525, H(5) \cdots F(3) 2.710 Å].

2.3. NLO properties

The values of first hyperpolarizability β measured in methanol solutions by the hyper-Rayleigh scattering (HRS) technique [23] for two compounds of this family showed no important increase of β as compared to the β value of the free nitrile ligands. Both $[\text{Ni}(\eta^5\text{-C}_5\text{H}_5)\{\text{P}(\text{C}_6\text{H}_5)_3\}(\text{p-NCC}_6\text{H}_4\text{N}(\text{CH}_3)_2)]\text{[PF}_6\text{]}$ and the free ligand $\text{NCC}_6\text{H}_4\text{N}(\text{CH}_3)_2$ itself have a value of β 18×10^{-30} esu, although a small increase of β with respect to the free ligand is found for $[\text{Ni}(\eta^5\text{-C}_5\text{H}_5)\{\text{P}(\text{C}_6\text{H}_5)_3\}(\text{p-NCC}_6\text{H}_4\text{C}_6\text{H}_5)]\text{[PF}_6\text{]}$ which showed a β value of 17×10^{-30} esu, twice the value of the free ligand *p*- $\text{NCC}_6\text{H}_4\text{C}_6\text{H}_5$ (8.7×10^{-30} esu). For both complexes and free nitrile ligands, a depolarization ratio of 0.20 ± 0.02 was found, as would be expected for a linear molecule with only one (diagonal) β tensor component. This suggests that β originates mainly from the conjugated path from metal to nitrile ligand and not for example in the PPh_3 ligand.

It would be expected that the increase of extension through the π system would rise the values of the second hyperpolarizability $\gamma(-3\omega; \omega, \omega, \omega)$, at least for the compound possessing the $\text{NCC}_6\text{H}_4\text{C}_6\text{H}_5$ coordinated ligand. Nevertheless this was not the case and it was found that all compounds of this family $[\text{Ni}(\eta^5\text{-C}_5\text{H}_5)\{\text{P}(\text{C}_6\text{H}_5)_3\}(\text{p-NCC}_6\text{H}_4\text{R})]\text{[PF}_6\text{]}$ (R = NH_2 , $\text{N}(\text{CH}_3)_2$, C_6H_5 , OCH_3 , H, F) measured at $\lambda = 1064$ nm, displayed a THG signal only slightly higher than the quartz background. This might be not surprising since experimental data did not give any evidence for such an extension as found for Ru(II) related compounds, where the metal centre was also involved on the extension of that π system through a back-donation mechanism [9], and the THG signal was quite significant ($\gamma(-3\omega; \omega, \omega, \omega)$ of 2.3×10^{-33} esu) [11].

2.4. Molecular orbital calculations

Extended Hückel molecular orbital calculations were performed on a model complex $[\text{Cp}(\text{PH}_3)\text{Ni}(\text{N}\equiv\text{CC}_6\text{H}_4\text{NH}_2)]^+$ having C_s symmetry, in order to understand the bonding mode of the nitrile ligand to the metallic fragment and its consequences upon the structural features of the complex. The interaction diagram between the nitrile ligand and the $\text{Cp}(\text{PH}_3)\text{Ni}^+$ cation is shown in Fig. 3.

Before analysing the diagram in detail, we can start by looking at the frontier orbitals of $\text{N}\equiv\text{CC}_6\text{H}_4\text{NH}_2$, drawn in Fig. 4. These can be grouped in one set of cylindrically symmetric σ orbitals (with respect to the Ni–N bond) and two sets of π orbitals in orthogonal planes. The latter descend from the interactions of the $\text{N}\equiv\text{C}$ π and π^* orbitals with the π and σ orbitals of the arene (π_{\perp} and π_{\parallel} MOs, respectively). The π_{\perp} set is orthogonal to the plane of the arene and therefore combines with the arene π orbitals, giving rise to combinations having bonding, non-bonding and antibonding characters relative to the C–C junction between the arene and the nitrile groups (notice the relevant orbitals π_{\perp} , $\pi_{\perp\text{nb}}$, and π_{\perp}^* in Fig. 4). The $\text{N}\equiv\text{C}$ π_{\parallel} parallel set can only combine with arene σ orbitals (p_{\parallel} and p_{\parallel}^* in Fig. 4, for instance).

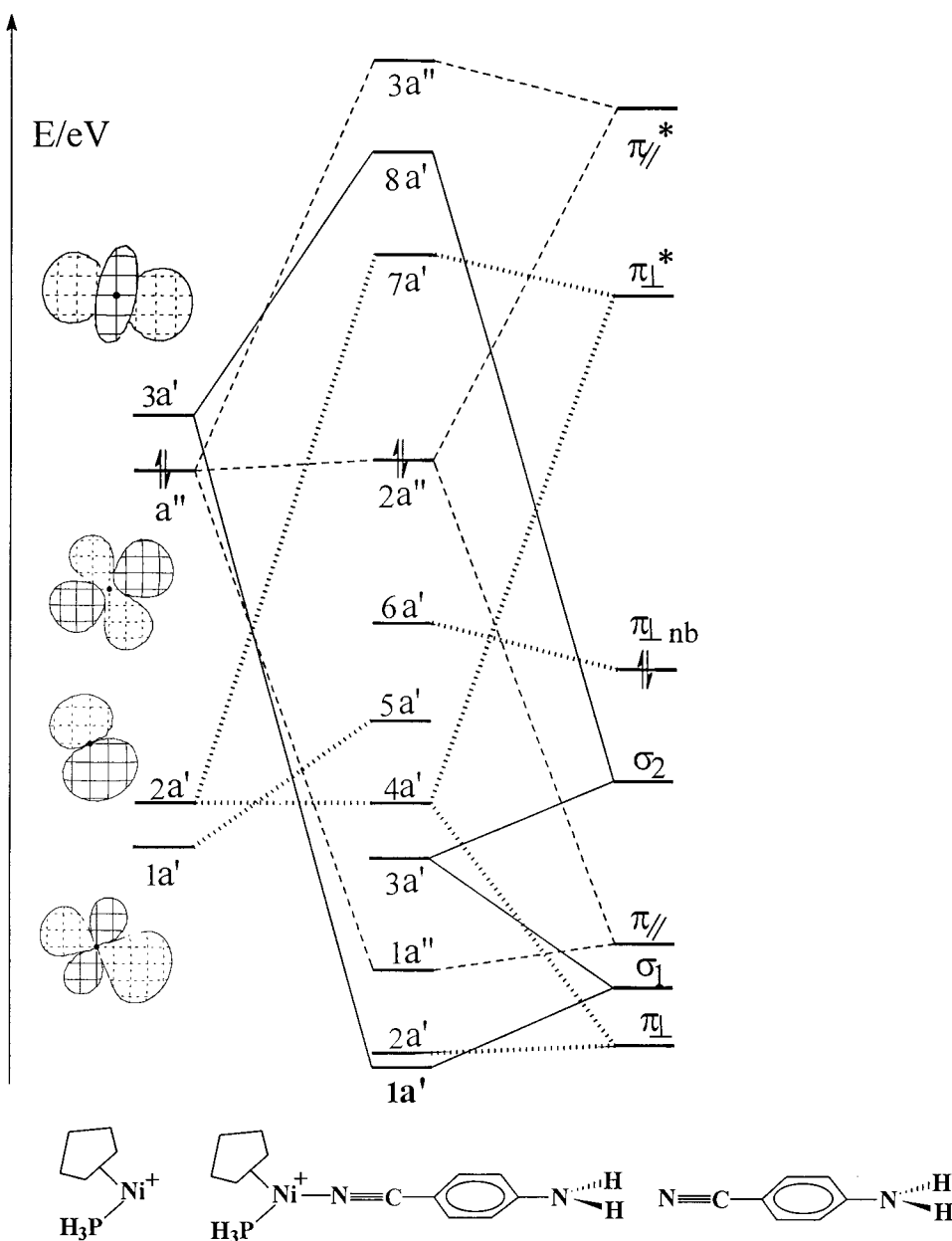


Fig. 3. Interaction diagram between the $\text{Cp}(\text{PH}_3)\text{Ni}^+$ cation and the nitrile $\text{N}\equiv\text{CC}_6\text{H}_4\text{NH}_2$.

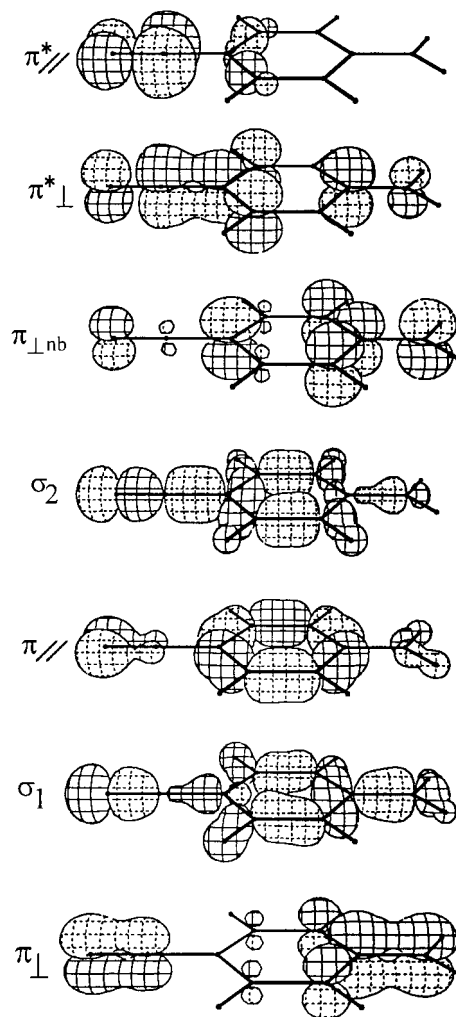


Fig. 4. CACAO three-dimensional representation of the frontier orbitals of $\text{N}\equiv\text{CC}_6\text{H}_4\text{NH}_2$.

Finally, two orbitals having σ character on the nitrile nitrogen atom are represented in Fig. 4 (σ_1 and σ_2 , respectively). As a matter of fact, the most important bonding component between the ligand and the nickel fragment is the combined s donation mainly from the latter σ_1 and σ_2 nitrile components into the empty $3a'$ orbital of the d^8 Ni(II) center (see Fig. 3). This interaction is represented by the thin solid line in the diagram and is responsible for the greatest part of the stabilization of the molecule relative to the two isolated fragments. While it is evident from the Fig. 4 that both the σ_1 and σ_2 orbitals are bonding between the atoms C and N of the ligand, it must be mentioned here some involvement of a third ligand orbital of σ symmetry (not shown), namely the low and filled antibonding combination between the carbon and nitrogen s orbitals. Importantly, the latter contribution nicely account for the strengthening of the $\text{N}\equiv\text{C}$ bond upon coordination to the metal atom. This trend, curiously pointed out at the experimental level (see above), is nicely reflected in the increase of $\text{N}\equiv\text{C}$ overlap population when the free and the coordinated ligand molecules are compared (1.675 vs. 1.744). A careful analysis indicates that the effect does not have a prevailing π -nature (vide infra) but can be traced to a certain depopulation of the low lying NC σ^* level also involved into the σ donation to the metal atom.

Still the major π interactions need to be underlined. Some of the occupied d levels are clearly interacting with both the π_{\perp} and the π_{\parallel} sets of nitrile ligand. In any case, both the π and π^* NC combinations are simultaneously involved. The resulting MOs are given by a linear combination of $a'' + \lambda_1\pi_{\parallel} + \lambda_2\pi_{\parallel}^*$, in such a way that the final molecular orbital is virtually nonbonding between the N and C atoms (Fig. 5). However, the interaction with π_{\parallel} is slightly stronger than with π_{\parallel}^* , making the global interaction a very weak π donation from the nitrile to the metal, instead of backdonation.

The interesting feature of the frontier π MOs is that they are not totally delocalized from the nickel atom to the NH_2 end, as either the C or the N atom of the nitrile does not contribute to them. This may be important in connection to the NLO properties.

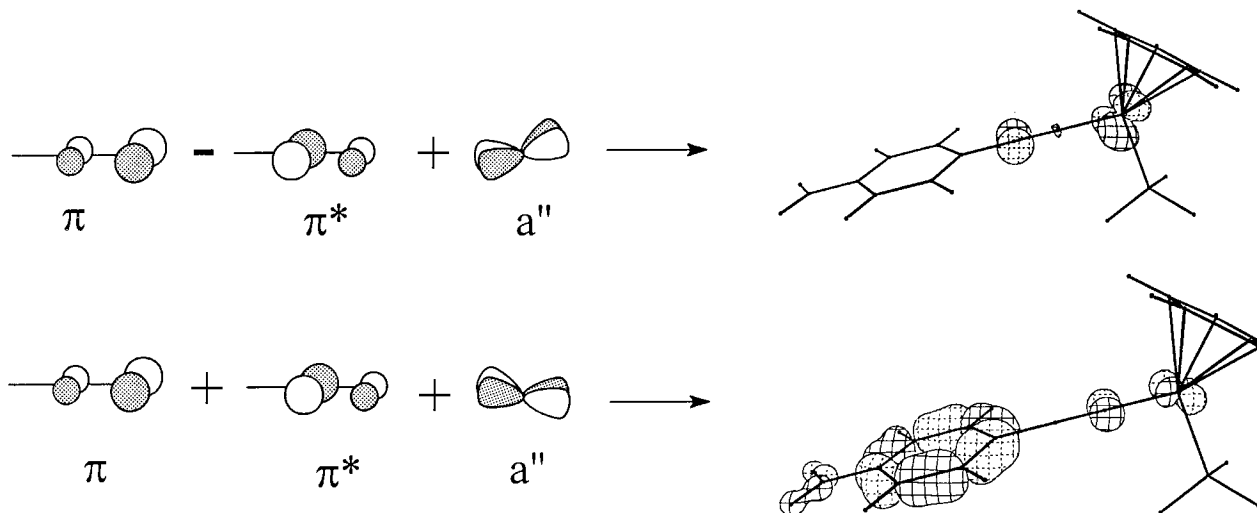


Fig. 5. The bonding and 'nonbonding' orbital resulting from the interaction between π and π^* and one orbital of the $\text{Cp}(\text{PH}_3)\text{Ni}^+$ fragment.

Recently calculations by Whitaker et al. [24] suggested a correlation between the hyperpolarizability and the HOMO–LUMO gap in a given molecule. The complex $[\text{Cp}(\text{PH}_3)\text{Ni}(\text{N}\equiv\text{CC}_6\text{H}_4\text{-NH}_2)]^+$ exhibits a large HOMO–LUMO gap (3.0 eV), which decreases when going to $[\text{Cp}(\text{PH}_3)\text{Ni}(\text{N}\equiv\text{CC}_6\text{H}_4\text{C}_6\text{H}_5)]^+$ (1.5 eV) and even more to $[\text{Cp}(\text{PH}_3)\text{Ni}(\text{N}\equiv\text{CC}_6\text{H}_4\text{NO}_2)]^+$ (0.4 eV), according to our calculations, though the nature of both HOMO and LUMO remains similar. In the latter two complexes, the LUMO has a lower energy as in comparison with the π^*_\perp orbital, reported in Fig. 4, the arene's contribution is larger. Moreover the presence of the nitro group is stabilizing (notice by contrast the antibonding and destabilizing effect of the NH_2 substituent). Ultimately, we might expect that the nitro derivative, with the smallest HOMO–LUMO gap, could be the best candidate for second harmonic generation. In this respect, also the unsubstituted phenyl derivative is expected to be better than the amino derivative.

2.5. Electrochemical studies

The electrochemical behaviour of this new family of compounds was investigated in acetonitrile and dichloromethane by cyclic voltammetry, with tetrabutylammonium hexafluorophosphate salt as supporting electrolyte, and showed both oxidative and reductive processes. The electrochemical studies discussed below for $[\text{Ni}(\eta^5\text{-C}_5\text{H}_5)\{\text{P}(\text{C}_6\text{H}_5)_3\}(\text{NCC}_6\text{H}_4\text{NH}_2)]\text{PF}_6$, typify the general behaviour of these nitrile nickel derivatives. The oxidative electrochemistry presented one single anodic wave ($E_{p_a} \sim +1.25$ V (acetonitrile), $E_{p_a} \sim +0.94$ V (dichloromethane)), without the cathodic counterpart, assigned to the irreversible oxidation of coordinated $\text{P}(\text{C}_6\text{H}_5)_3$ and $\text{NCC}_6\text{H}_4\text{NH}_2$ ligands, by comparison with their electrochemical behaviour as uncoordinated compounds. The reductive electrochemistry was somehow more complex and a set of experiments had to be carried out in order to understand the overall process. In fact, when the solvent was CH_2Cl_2 , only one cathodic wave at $E_{p_c} \sim -1.1$ V was observed without the anodic counterpart, which slightly emerged, as the temperature went down to $\approx -30^\circ\text{C}$. However, equivalent studies in acetonitrile showed a more complex set of results associated to the reductive electrochemistry of these compounds as shown on Fig. 6 (line a).

At room temperature, a broad cathodic process suggesting overlap of two waves with maxima at $E_{p_c} \sim -0.83$ V (A) was found, followed by a second cathodic wave at $E_{p_c} \sim -1.04$ V (B). Both processes presented very broad anodic counterparts. An additional, quasi-reversible, weak redox wave C at $E_{p_{1/2}} = 0.08$ V was also observed in all voltammograms independently of the potential scan direction, but its intensity was found to be higher immediately after reversing the potential at -1.5 V. This wave C was assigned to a small amount of nickelocene, formed in situ, according to the mechanism discussed below. Experiments with decrease of temperature showed that when temperature went down to -30°C the first cathodic wave A became sharper, the wave B became relatively less intensive, and simultaneously both corresponding anodic counterparts emerged clearer as can be observed on line b of Fig. 6. These observations suggested that the broadness of wave A might be related to any possible decomposition product of the reduced $[\text{Ni}^1(\eta^5\text{-C}_5\text{H}_5)\{\text{P}(\text{C}_6\text{H}_5)_3\}(\text{NCC}_6\text{H}_4\text{NH}_2)]$ nineteen electron species, this process being slower at lower temperatures, as would be expected and was found at -30°C . Addition of excess of $\text{NCC}_6\text{H}_4\text{R}$ (10 times the initial nickel compound concentration) did not show any significant difference on the voltammogram. However, if the same excess of PPh_3 was added to the parent solution, only a new quasi-reversible redox wave was found in the voltammogram, at $E_{p_{1/2}} = -0.66$ V ($\Delta E = 90$ mV), and it was assigned to the reduction of the $[\text{Ni}(\eta^5\text{-$

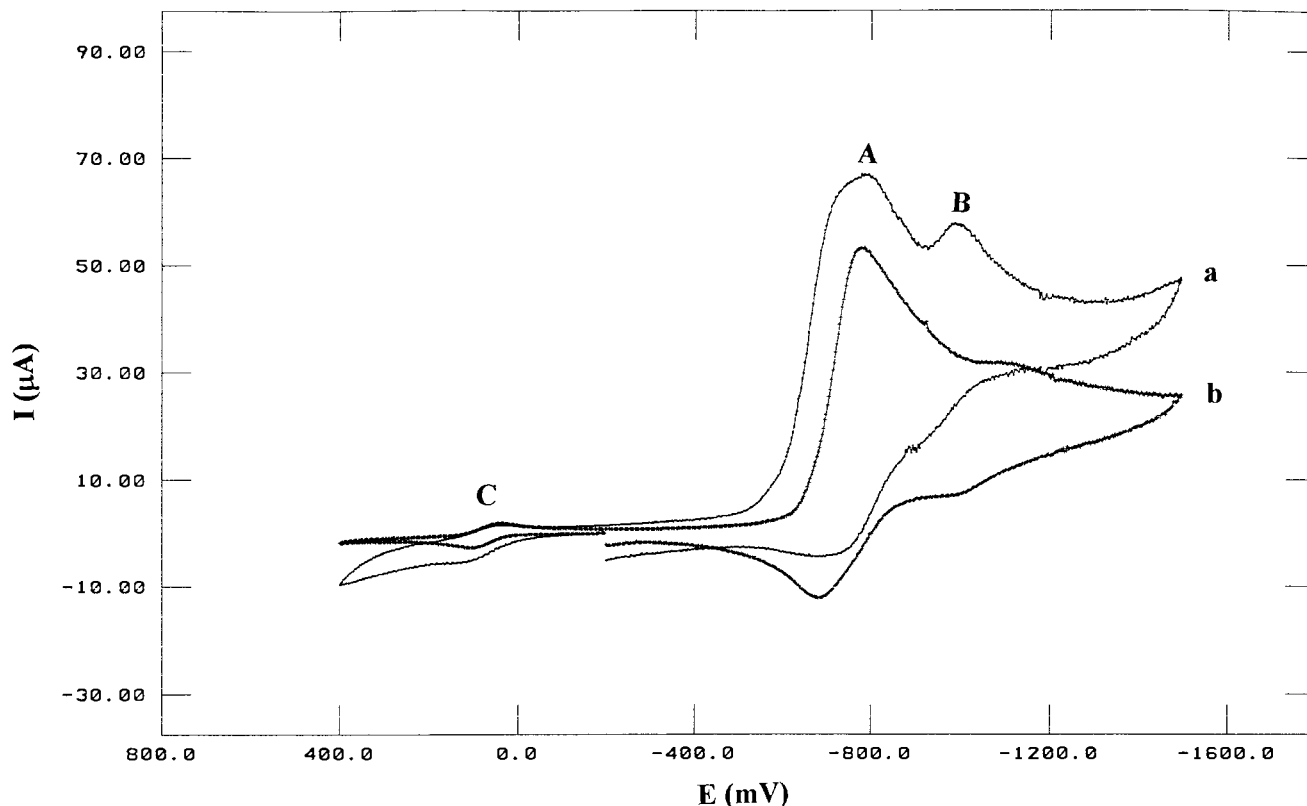
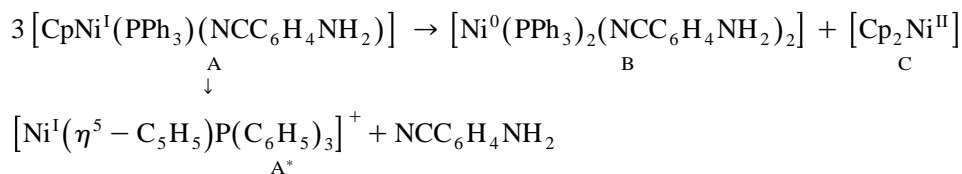


Fig. 6. Cyclic voltammogram of compound $[\text{Ni}(\eta^5\text{-C}_5\text{H}_5)(\text{P}(\text{C}_6\text{H}_5)_3)(\text{NCC}_6\text{H}_4\text{NH}_2)]\text{PF}_6$, 10^{-3} M in acetonitrile, at scan rate of 200 mV s^{-1} on $0.1 \text{ M } [(\text{Bu}^n)_4\text{N}][\text{PF}_6]/\text{CH}_3\text{CN}$ solution vs. wire Ag reference. (a) room temperature; (b) -30°C .

$\text{C}_5\text{H}_5)(\text{P}(\text{C}_6\text{H}_5)_3)_2]^+$ new species, formed in the electrochemical cell by a metathesis chemical reaction, due to the large excess of phosphine, as was proved in a separate chemical reaction carried out on the bench. Therefore, electrochemical studies on compound $[\text{Ni}(\eta^5\text{-C}_5\text{H}_5)(\text{P}(\text{C}_6\text{H}_5)_3)_2]\text{PF}_6$ were found to be necessary. In fact, under the same experimental conditions, an analogous pattern was found for the voltammogram of this compound and again the very first irreversible reduction broad wave showed up at $E_{p_c} \sim -0.83 \text{ V}$. Nevertheless, with the presence of large excess of $\text{P}(\text{C}_6\text{H}_5)_3$ in solution, only a new quasi-reversible redox process at $E_{p_{1/2}} = -0.68 \text{ V}$ was found. This observation suggested that the nineteen unstable reduced species, led to the decoordination of one $\text{P}(\text{C}_6\text{H}_5)_3$ ligand in the present case, and to the decoordination of the more labile $\text{NCC}_6\text{H}_4\text{NH}_2$ ligand, in our nickel nitrile derivative with formation in both cases, of a $[\text{Ni}^I(\eta^5\text{-C}_5\text{H}_5)(\text{P}(\text{C}_6\text{H}_5)_3)]^+$ new species (A* on the scheme below), whose reduction would be responsible for the broadness on the first reduction wave. In addition, other decomposition products might be formed leading to the presence of Ni^0 and Ni^{II} derivatives, responsible for wave B and the increased amount of nickelocene associated to wave C.

Our results are in good agreement with other studies published in the literature [25] according to which the following reactions are suggested:



According to our calculations, reduction of the complex should lead to population of the Ni–N antibonding LUMO, resulting in loss of the nitrile ligand.

2.6. Electronic spectra

Electronic spectra of complexes $[\text{Ni}(\eta^5\text{-C}_5\text{H}_5)(\text{P}(\text{C}_6\text{H}_5)_3)(\text{NCC}_6\text{H}_4\text{R})]\text{PF}_6$ were recorded in 1.7×10^{-5} M in dichloromethane, methanol and chloroform solutions, in the range of wavelengths 200–1000 nm. All the compounds

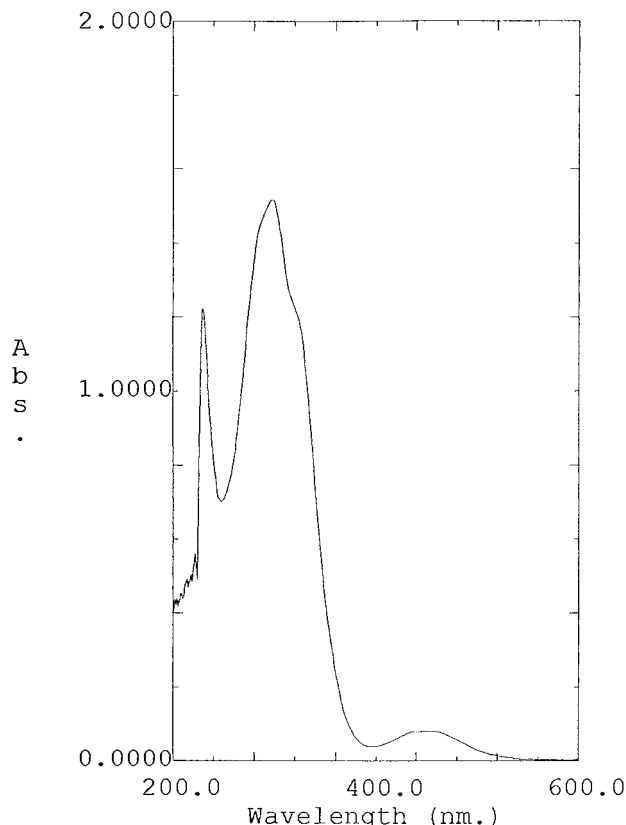


Fig. 7. Electronic spectra of compound $[\text{Ni}(\eta^5\text{-C}_5\text{H}_5)\{\text{P}(\text{C}_6\text{H}_5)_3\}(\text{NCC}_6\text{H}_4\text{NH}_2)]\text{[PF}_6\text{]} (1.7 \times 10^{-5} \text{ M in dichloromethane})$.

presented two intense absorption bands on the UV region attributed to electronic transitions occurring in the aromatic ligands, and also one band in the visible region where d–d transitions are expected to occur. Fig. 7 recorded for compound $[\text{Ni}(\eta^5\text{-C}_5\text{H}_5)\{\text{P}(\text{C}_6\text{H}_5)_3\}(\text{NCC}_6\text{H}_4\text{NH}_2)]\text{[PF}_6\text{]}$ typifies the electronic spectra, obtained in solutions of dichloromethane.

Band at 228–235 nm ($\epsilon = 1.8 \times 10^4 \text{ l mol}^{-1} \text{ cm}^{-1}$) was attributed to transitions occurring in the fragment $[\text{Ni}(\eta^5\text{-C}_5\text{H}_5)\{\text{P}(\text{C}_6\text{H}_5)_3\}]$ by comparison with the electronic spectra of $[\text{Ni}(\eta^5\text{-C}_5\text{H}_5)\{\text{P}(\text{C}_6\text{H}_5)_3\}_2]\text{[PF}_6\text{]}$. The absorption band at 296 nm ($\epsilon = 3.2 \times 10^4 \text{ l mol}^{-1} \text{ cm}^{-1}$) was attributed to the coordinated $\text{NCC}_6\text{H}_4\text{NH}_2$ nitrile, which in the free ligand occurs at 269 nm ($\epsilon = 2.2 \times 10^4 \text{ l mol}^{-1} \text{ cm}^{-1}$) in the same solvent. The band in the visible, occurring at 451 nm ($\epsilon = 1.3 \times 10^3 \text{ l mol}^{-1} \text{ cm}^{-1}$) was attributed to d–d transitions (for some compounds of this family a shoulder at lower wavelength was also observed both in dichloromethane and methanol). The presence of this band on the electronic spectra of $[\text{Ni}(\eta^5\text{-C}_5\text{H}_5)\{\text{P}(\text{C}_6\text{H}_5)_3\}_2]\text{[PF}_6\text{]}$ and $[\text{Ni}(\eta^5\text{-C}_5\text{H}_5)\{\text{P}(\text{C}_6\text{H}_5)_3\}\text{Cl}]\text{[PF}_6\text{]}$ precludes its assignment to any nitrile–metal charge transfer. Therefore, the CT transition relative to the nitrile might be the responsible for the quadratic response observed on the complexes.

3. Concluding remarks

The new compounds $[\text{Ni}(\eta^5\text{-C}_5\text{H}_5)\{\text{P}(\text{C}_6\text{H}_5)_3\}\text{NCC}_6\text{H}_4\text{R}]\text{[PF}_6\text{]}$ where R is a donor group (NH_2 , $\text{N}(\text{CH}_3)_2$, C_6H_5 , OCH_3 , H, F) showed no interesting SHG or THG signals, though they apparently obeyed the required structural conditions, exhibiting an Acceptor- π system-Donor arrangement. In fact, crystal structure determination of the NH_2 derivative showed an almost planar geometry for the substituted nitrile and our studies by the hyper-Rayleigh scattering technique suggest that β originates mainly from the conjugated path from metal to nitrile ligand. A reasonable explanation for the absence of NLO properties was provided by our theoretical studies which suggested the σ donation of nitrile to nickel to be the most significant component of the bonding and that π interaction had a net negligible effect on the delocalization.

4. Experiment

All experiments were carried out under nitrogen by the use of standard Schlenk-tube techniques. Solvents were purified according to the usual methods [26]. Solid state IR spectra were measured on a Perkin-Elmer 457 spectrophotometer with KBr pellets; only significant bands are cited in the text. ^1H and ^{31}P NMR spectra were recorded on a Bruker CXP 300 spectrometer, and ^{13}C NMR spectra were recorded on a Varian Unity 300 spectrometer at probe temperature. Microanalyses were performed, in our laboratories, using a Fisons Instruments EA1108 system. Data acquisitions, integration and handling were performed using a PC with the software package Eager-200 (Carlo Erba Instruments). Melting points were obtained using a Reichert Thermovar. Electronic spectra were recorded using dried solvents at room temperature, on a Shimadzu UV-1202.

The ^1H (acetone- d_6) and ^{13}C (chloroform- d) chemical shifts are reported in parts per million downfield from internal Me_4Si and ^{31}P NMR spectra are reported in parts per million downfield from external 85% H_3PO_4 .

4.1. Preparation of $[\text{Ni}(\eta^5\text{-C}_5\text{H}_5)\{\text{P}(\text{C}_6\text{H}_5)_3\}\text{Cl}]$

This starting material was prepared following the process described in the literature [27].

4.2. Preparation of $[\text{Ni}(\eta^5\text{-C}_5\text{H}_5)\{\text{P}(\text{C}_6\text{H}_5)_3\}(\text{NCC}_6\text{H}_4\text{R})][\text{PF}_6]$

All the complexes were prepared by the process described as follows. A solution of $[\text{Ni}(\eta^5\text{-C}_5\text{H}_5)\{\text{P}(\text{C}_6\text{H}_5)_3\}\text{Cl}]$ (1 mmol) in diethyl ether (~ 150 ml), was added dropwise, to a solution of nitrile $\text{NCC}_6\text{H}_4\text{R}$ (≈ 10 mmol) in the same solvent (20 ml) containing TIPF_6 (1.5 mmol) in suspension, at room temperature with stirring. A brown solid precipitates immediately together with simultaneous precipitation of TiCl_4 . The mixture was allowed to stir for 2 h. After filtration, the solid residue was washed several times with diethyl ether to remove the excess of unreacted nitrile. The residue was then dissolved in chloroform and filtrated, leaving behind the insoluble TiCl_4 . After concentration of this solution and addition of ether, brown–green crystals of the new compound nicely precipitate. Crystals for X-ray measurements can be grown by slow diffusion vapor of ether in a concentrated dichloromethane solution of the required compound.

$[\text{Ni}(\eta^5\text{-C}_5\text{H}_5)\{\text{P}(\text{C}_6\text{H}_5)_3\}(\text{NCC}_6\text{H}_4\text{NH}_2)][\text{PF}_6]$: Yield: 70%; Anal. Found: C, 55.4; H, 4.1; N, 4.3. $\text{C}_{30}\text{H}_{26}\text{N}_2\text{P}_2\text{F}_6\text{Ni}$; Calc. C, 55.5; H, 4.0; N, 4.3. M. p.: 173°C (d). $[\text{Ni}(\eta^5\text{-C}_5\text{H}_5)\{\text{P}(\text{C}_6\text{H}_5)_3\}(\text{NCC}_6\text{H}_4\text{N}(\text{CH}_3)_2)][\text{PF}_6]$: Yield: 95%; Anal. Found: C, 57.0; H, 4.5; N, 4.2. $\text{C}_{32}\text{H}_{30}\text{N}_2\text{P}_2\text{F}_6\text{Ni}$; Calc. C, 56.8; H, 4.5; N, 4.1. M. p.: 167°C (d). $[\text{Ni}(\eta^5\text{-C}_5\text{H}_5)\{\text{P}(\text{C}_6\text{H}_5)_3\}(\text{NCC}_6\text{H}_4\text{C}_6\text{H}_5)][\text{PF}_6]$: Yield: 85%; Anal. Found: C, 59.6; H, 4.0; N, 2.0. $\text{C}_{36}\text{H}_{29}\text{NP}_2\text{F}_6\text{Ni}$; Calc. C, 60.5; H, 4.1; N, 2.0. M. p.: 104°C . $[\text{Ni}(\eta^5\text{-C}_5\text{H}_5)\{\text{P}(\text{C}_6\text{H}_5)_3\}(\text{NCC}_6\text{H}_4\text{OCH}_3)][\text{PF}_6]$: Yield: 95%; Anal. Found: C, 55.8; H, 4.1; N, 2.2. $\text{C}_{31}\text{H}_{27}\text{NOP}_2\text{F}_6\text{Ni}$; Calc. C, 56.1; H, 4.1; N, 2.1. M. p.: 170°C . $[\text{Ni}(\eta^5\text{-C}_5\text{H}_5)\{\text{P}(\text{C}_6\text{H}_5)_3\}(\text{NCC}_6\text{H}_5)][\text{PF}_6]$: Yield: 95%; Anal. Found: C, 56.5; H, 3.9; N, 2.1. $\text{C}_{30}\text{H}_{25}\text{NP}_2\text{F}_6\text{Ni}$; Calc. C, 56.8; H, 4.0; N, 2.2. M. p.: 159°C . $[\text{Ni}(\eta^5\text{-C}_5\text{H}_5)\{\text{P}(\text{C}_6\text{H}_5)_3\}(\text{NCC}_6\text{H}_4\text{F})][\text{PF}_6]$: Yield: 90%; Anal. Found: C, 54.9; H, 3.8; N, 2.1. $\text{C}_{30}\text{H}_{24}\text{NP}_2\text{F}_7\text{Ni}$; Calc. C, 55.2; H, 3.7; N, 2.1. M. p.: 164°C (d).

4.3. X-ray measurements

Intensities were measured on an Enraf-Nonius CAD4 diffractometer using graphite monochromated $\text{MoK}\alpha$ radiation (0.71069 \AA). Cell dimensions were determined from the measured θ values for 25 intense reflections with $12 \leq \theta \leq 15.5^\circ$. 8260 reflection intensities, of which 6305 were independent, were measured by the ω - 2θ scan mode, in the range $1.7 \leq \theta \leq 27.0^\circ$. Data were corrected for Lorentz and polarization effects. The compound $\text{C}_{30}\text{H}_{26}\text{N}_2\text{P}_2\text{F}_6\text{Ni}$; Mr = 649.2, crystallizes in the monoclinic space group; $P2_1/n$; with cell dimensions $a = 9.354(2) \text{ \AA}$, $b = 14.600(3) \text{ \AA}$, $c = 21.589(6) \text{ \AA}$, $\beta = 101.31(2)^\circ$; $V = 2891.1(12) \text{ \AA}^3$; $Z = 4$; $D_c = 1.491 \text{ g cm}^{-3}$ and $\mu(\text{MoK}\alpha) = 8.44 \text{ cm}^{-1}$.

The structure was solved by a combination Patterson and difference Fourier syntheses using programs SHELX86 [28] and SHELX93 [29]. All non hydrogen atoms and the two amino hydrogen atoms were found in the difference maps. The non-hydrogen atoms were refined anisotropically. The localized hydrogen atoms were refined isotropically with a restrained N–H distance of 0.86 \AA . The remaining hydrogen atoms were placed in calculated positions and refined with group isotropic thermal parameters (one U_{iso} for the Ph ring of the phosphine, one U_{iso} for the Cp ring, and one U_{iso} for the Ph ring of the nitrile ligand). In the final refinement the R_1 and wR_2 obtained were 0.063 and 0.157 for $I > 2\sigma(I)$ and 378 refined parameters. The R indices using all data were $R_1 = 0.089$ and $wR_2 = 0.1897$ with a goodness of fit of $s = 1.058$.

Final atomic positional coordinates for the non-hydrogen atoms are given in Table 4. Anisotropic thermal

Table 4

Atomic coordinates ($\times 10^4$), and equivalent isotropic displacement parameters ($\text{\AA}^2 \times 10^3$), for $[\text{Ni}(\eta^5\text{-C}_5\text{H}_5)\{\text{P}(\text{C}_6\text{H}_5)_3\}(\text{NCC}_6\text{H}_4\text{NH}_2)]\text{PF}_6$. U_{eq} , is defined as one third of the trace of the orthogonalized U_{ij} tensor

| | x | y | z | U_{eq} |
|--------|-----------|----------|---------|-----------------|
| Ni(1) | 13(1) | 1990(1) | 2199(1) | 37(1) |
| P(1) | 229(1) | 1162(1) | 1386(1) | 33(1) |
| C(1) | -830(4) | 1642(3) | 664(2) | 39(1) |
| C(2) | -1849(4) | 1142(3) | 253(2) | 48(1) |
| C(3) | -2581(5) | 1563(4) | -297(2) | 66(1) |
| C(4) | -2272(6) | 2444(4) | -436(2) | 66(1) |
| C(5) | -1268(6) | 2937(3) | -27(2) | 61(1) |
| C(6) | -559(5) | 2537(3) | 526(2) | 51(1) |
| C(7) | 2031(4) | 965(3) | 1206(2) | 38(1) |
| C(8) | 3065(5) | 517(3) | 1640(2) | 52(1) |
| C(9) | 4447(5) | 369(4) | 1527(2) | 64(1) |
| C(10) | 4776(5) | 647(4) | 969(3) | 72(2) |
| C(11) | 3771(6) | 1089(4) | 531(3) | 77(2) |
| C(12) | 2379(5) | 1247(3) | 640(2) | 57(1) |
| C(13) | -482(4) | 24(3) | 1464(2) | 37(1) |
| C(14) | -1413(4) | -116(3) | 1882(2) | 42(1) |
| C(15) | -1956(5) | -971(3) | 1957(2) | 52(1) |
| C(16) | -1590(5) | -1695(3) | 1611(3) | 60(1) |
| C(17) | -657(6) | -1569(3) | 1201(3) | 67(1) |
| C(18) | -117(5) | -706(3) | 1124(2) | 57(1) |
| N(1) | -1834(4) | 2426(3) | 1855(2) | 51(1) |
| C(21) | -2919(5) | 2725(3) | 1628(2) | 52(1) |
| C(22) | -4258(4) | 3129(3) | 1326(2) | 51(1) |
| C(23) | -5380(5) | 3278(4) | 1646(2) | 57(1) |
| C(24) | -6630(5) | 3710(4) | 1351(2) | 59(1) |
| C(25) | -6797(4) | 3997(3) | 731(2) | 55(1) |
| C(26) | -5674(5) | 3832(4) | 407(2) | 71(2) |
| C(27) | -4429(5) | 3402(4) | 702(2) | 71(2) |
| N(2) | -8034(5) | 4434(4) | 440(3) | 83(2) |
| C(111) | 2111(5) | 2009(4) | 2722(2) | 62(1) |
| C(112) | 1512(6) | 2842(3) | 2808(2) | 63(1) |
| C(113) | 292(6) | 2668(4) | 3058(2) | 71(2) |
| C(114) | 213(6) | 1722(5) | 3184(2) | 71(2) |
| C(115) | 1311(6) | 1324(4) | 2966(2) | 65(1) |
| P(2) | 9075(1) | 5403(1) | 1504(1) | 52(1) |
| F(1) | 7845(6) | 5979(4) | 1124(2) | 155(2) |
| F(3) | 10,134(7) | 5956(4) | 1183(3) | 172(3) |
| F(4) | 8110(7) | 4853(4) | 1838(3) | 184(3) |
| F(2) | 8949(5) | 4698(3) | 952(2) | 115(1) |
| F(5) | 10,425(6) | 4886(4) | 1878(2) | 158(2) |
| F(6) | 9259(6) | 6123(3) | 2052(2) | 120(2) |

parameters for the non-hydrogen atoms, atomic positional and thermal parameters for hydrogen atoms and a list of observed and final calculated structure factors are available as supplementary material. Drawings were made with the program ORTEPH [16] and SCHAKAL [15]. Atomic scattering values were taken from the International Tables of X-ray Crystallography [30].

4.4. β measurements

Because the usual EFISHG (electric field induced second harmonic generation) technique for determination of $\mu\beta$ is not applicable for these compounds, the hyper-Rayleigh scattering technique was used, which does not require any static field to be applied.

HRS measurements with a fundamental wavelength of 1.064 μm were performed on dilute solutions (in the order of 1 mg/ml) in methanol. The solutions were systematically passed through 500 nm microporous filters. Laser pulses (energy: $\sim 20 \mu\text{J}$, width: 70 ps, repetition rate 2 kHz) from a Nd:YAG regenerative amplifier were focused into a rectangular glass cell by a 100 mm lens. The scattered harmonic light was collected at 90° and filtered by a monochromator with 1 nm bandwidth. Single photon pulses from a photomultiplier were detected in a 5 ns time gate

around the laser pulse. The count rates were corrected for pile-up errors at increasing count gates. Systematic scanning of a narrow region around 532 nm showed no significant photoluminescence background. In a reference arm a fraction of the laser light was frequency-doubled and this intensity was used to correct for slow laser fluctuations. Using the internal reference method we obtain the ratio $\beta_{\text{HRS(solute)}}/\beta_{\text{HRS(solvent)}}$, where β_{HRS} is given in terms of the oriental averages $\langle \beta_{IJK}^2 \rangle$ of the molecular hyperpolarizability by $\sqrt{(\langle \beta_{ZZZ}^2 \rangle + \langle \beta_{XZZ}^2 \rangle)}$. Applying the previously used approximation [23] that the β tensor of the solvent molecules is also dominated by β_{ZZZ} and adopting β values of 0.49×10^{-30} esu for chloroform [31] and 0.23×10^{-30} esu for methanol [31], the β value for the solute ($=|\beta_{ZZZ}|$) was determined. We measured this β value of methanol by external reference relative to chloroform, using the usual Lorentz local field factors and correcting for the different refraction by both solvents. The incident power had to be reduced to less than 20 mW (10 μ J per pulse) during the external reference measurements to minimize thermal lensing effects in methanol.

4.5. THG measurements

THG measurements of the thin films were carried out using the Maker fringe technique [32] employing a 10 pps Q-switched ND:YAG laser operating at 1064 nm with a pulse duration of 10 ns and a pulse energy at the sample of at most 140 μ J. The fundamental beam was directed through filters and polarizing optics before it was focused on the sample by a 300 mm lens. The sample was mounted on a rotation stage so that the angle of incidence of the laser beam could be varied, with the film side of the sample facing the detector. The polarization of the electrical field was parallel to the rotation axis and care was taken that the incident beam and the rotation axis coincided. The third harmonic beam at 355 nm was detected in a transmission geometry using a photomultiplier connected to a photon counter. In order to block other wavelengths, a monochromator was used. A personal computer was used to control the rotation stage and collect the data. Each data point was obtained by sampling signals from 300 laser pulses.

Maker fringes were recorded in the range -30° to $+30^\circ$ with respect to normal incidence of the laser beam. The fringe patterns of a sample consisting of a thin film on a fused silica substrate were first recorded, then after removal of the thin film, in situ, Maker fringes of the bare substrate were recorded in the same range.

4.6. Molecular orbital calculations

All the molecular orbital calculations were done using the extended Hückel method [33–35] with modified H_{ij} 's [36]. The basis set for the metal atom consisted of ns , np , and $(n-1)d$ orbitals. The s and p orbitals were described by single Slater-type wave functions, and the d orbitals were taken as contracted linear combinations of two Slater-type wave functions. Standard parameters were used for H, C, N, and O, while those for Ni were the following (H_{ii}/eV , ζ): 4s, -9.11 , 1.825; 4p, -5.15 , 1.125; 3d, -13.40 , 5.75, 2.000 (ζ_2), 0.5683 (C_1), 0.6292 (C_2). Three-dimensional representations of orbitals were drawn using the program CACAO [37].

An idealized model having C_s symmetry was built, based on the structure of the nickel complex described in this work. The following distances (Å) and angles ($^\circ$) were used: Ni–Cp 1.74, C–C 1.40, C–H 1.08, Ni–P 2.17, P–H 1.4, Ni–N 1.65, NC 1.13, N–H 1.0, C–N 1.35, Cp–Ni–P 133.0. The position of the nitrile ligand relative to the plane bisecting the Cp–Ni–P plane was optimized.

4.7. Electrochemical apparatus

The electrochemistry instrumentation consisted of a Potentiostat EG&A, Princeton Applied Research, Model 273A, and experiments were monitored in a personal computer loaded with Model 270 Electrochemical Analysis Software 3.00 of EG&A, Princeton Applied Research. Potentials were referred to a silver electrode which was checked with a 1.0×10^{-3} M solution of ferrocene in acetonitrile containing 0.10 M LiClO_4 for which the ferrocenium/ferrocene potential was in good agreement with the literature [38]. The working electrode was a 2-mm piece of platinum wire. The secondary electrode was a platinum wire coil. Cyclic voltammetry experiments were performed at room temperature in a PAR polarographic cell. Solutions studied were 1 mM in solute and 0.1 M in tetrabutylammonium hexafluorophosphate as supporting electrolyte.

The electrolyte was prepared from Bu_4NBr and KPF_6 (both purchased from Aldrich Chemical), recrystallized from ethanol, washed with diethyl ether, and dried in vacuum at room temperature for 24 h. Reagent grade acetonitrile and dichloromethane were dried over P_2O_5 and CaH_2 , respectively, and distilled before use under an argon atmosphere. An argon atmosphere was maintained over the solution during the experiment.

Acknowledgements

Financial support of this work was provided by Project STRDA/P/CEN/512/92 and EU Human Capital and Mobility Programme. Paulo Mendes thanks Junta Nacional de Investigação Científica e Tecnológica for Grant BD/2168/92-IC and support of his stay at the Danish Institute of Fundamental Metrology (DFM) at Copenhagen, Denmark. Authors deeply thank Dr. Jan Petersen at DFM, Dr. Thomas Bjornholm at the Center for Interdisciplinary Studies of Molecular Interactions (CISMI) at Copenhagen, and Dr. Tommy Geisler at Institut of Physics, Aalborg University, Denmark, for THG measurements and fruitful discussions. E.G. is Research Director of the Fund for Scientific Research of Flanders (FWO). The work in Antwerp is partly funded by the Flanders Government in its action for the promotion of participation in EU-research programmes.

References

- [1] D.J. Williams, *Angew. Chem. Int. Ed. Engl.* 23 (1984) 690, and refs. therein.
- [2] M.L.H. Green, S.R. Marder, M.E. Thompson, J.A. Bandy, D. Bloor, P.V. Kolinsky, R.J. Jones, *Nature* 330 (1987) 360.
- [3] S.R. Marder, J.W. Perry, B.G. Tiemann, W.P. Schaefer, *Organometallics* 10 (1991) 1896.
- [4] M. Kimura, H. Abdel-Halim, D.W. Robinson, D.O. Cowan, *J. Organomet. Chem.* 403 (1991) 365.
- [5] H.E. Bunting, M.L.H. Green, S.R. Marder, M.E. Thompson, D. Bloor, P.V. Kolinsky, R.J. Jones, *Polyhedron* 11 (1992) 1489.
- [6] J.C. Calabrese, L.-T. Cheng, J.C. Green, S.R. Marder, W. Tam, *J. Am. Chem. Soc.* 113 (1991) 7227.
- [7] H.S. Nalwa, *Appl. Organomet. Chem.* 5 (1991) 349.
- [8] N.J. Long, *Angew. Chem. Int. Ed. Engl.* 34 (1995) 21.
- [9] A.R. Dias, M.H. Garcia, M.P. Robalo, M.L.H. Green, K.K. Lai, A.J. Pulham, S.M. Kuebler, G. Balavoine, *J. Organomet. Chem.* 453 (1993) 241.
- [10] A.R. Dias, M.H. Garcia, J.C. Rodrigues, M.L.H. Green, S. Kuebler, *J. Organomet. Chem.* 475 (1994) 241.
- [11] A.R. Dias, M.H. Garcia, J.C. Rodrigues, J.C. Petersen, T. Bjornholm, T. Geisler, *J. Mater. Chem.* 5 (1995) 1861.
- [12] C. Combelas, H. Gautier, J. Simon, A. Thiebault, F. Tourmilhac, M. Barzoukas, D. Josse, I. Ledoux, C. Amatore, J.N. Verpeaux, *J. Chem. Soc. Chem. Commun.*, 1988, 203.
- [13] A. Dulcic, C. Sauteret, *J. Chem. Phys.* 69 (1978) 3453.
- [14] W.J. Geary, *Coord. Chem. Rev.* 7 (1977) 81.
- [15] E. Keller, SCHAKAL88, Graphical Representation of Molecular Models, Univ. of Freiburg, Germany.
- [16] C.K. Johnson, ORTEP II, A Fortran Thermal-ellipsoid Plot Program for Crystal Structure Illustrations, Report ORNL-5138, Oak Ridge National Laboratory, Oak Ridge, TN, 1976.
- [17] F.J. Lalor, T.J. Desmond, G. Ferguson, P.Y. Siew, *J. Chem. Soc., Dalton Trans.* (1982) 1981.
- [18] F.H. Allen, J.E. Davies, J.J. Galoy, O. Kennard, C.F. Macrae, E.M. Mitchell, G.F. Mitchell, J.M. Smith, D.G. Watson, *J. Chem. Info. Comp. Sci.* 31 (1991) 187.
- [19] W. Bassi, C. Benedicenti, M. Calcaterra, G. Rucci, *J. Organomet. Chem.* 117 (1976) 285.
- [20] W. Bassi, C. Benedicenti, M. Calcaterra, R. Intrito, G. Rucci, C. Santini, *J. Organomet. Chem.* 144 (1978) 225.
- [21] S. Merlino, F. Sartori, *Acta Crystallogr. B* 38 (1982) 1476.
- [22] A. Heine, R. Herbst-Irmer, D. Stalke, W. Kühnle, K.A. Zachariasse, *Acta Crystallogr. B* 50 (1994) 363.
- [23] K. Clays, A. Persoons, *Phys. Rev. Lett.* 66 (1991) 2980.
- [24] C.M. Whitaker, E.V. Patterson, K.L. Kott, R.J. McMahon, *J. Am. Chem. Soc.* 118 (1996) 9966.
- [25] E. Kent Barefield, D.A. Krost, D.S. Edwards, D.G. Van Derveer, R.L. Trytko, S.P. O'Rear, *J. Am. Chem. Soc.* 103 (1981) 6219.
- [26] D.D. Perrin, W.I.F. Amarego, D.R. Perrin, *Purification of Laboratory Chemicals*, 2nd edn., Pergamon, New York, 1980.
- [27] K.W. Barnett, *J. Chem. Educ.* 51 (1974) 422.
- [28] G.M. Sheldrick, SHELX86, in: *Crystallographic Computing 3*, G.M. Sheldrick, C. Krüger, R. Goddard (Eds.), Oxford Univ. Press, 1985.
- [29] G.M. Sheldrick, SHELX93, Program for Crystal Structure Determination, Univ. of Göttingen, Göttingen, Germany, 1993.
- [30] *International Tables for X-Ray Crystallography*, Vol. 4 Kynoch Press, Birmingham, 1974.
- [31] F. Kajzar, I. Ledoux, Z. Ziss, *Phys. Rev. A* 36 (1987) 2210.
- [32] F. Kajzar, J. Messier, C. Rosilio, *J. Appl. Phys.* 60 (1986) 3040.
- [33] R. Hoffmann, *J. Chem. Phys.* 39 (1986) 1397.
- [34] R. Hoffmann, W.N. Lipscomb, *J. Chem. Phys.* 36 (1962) 2179.
- [35] R. Hoffmann, W.N. Lipscomb, *J. Chem. Phys.* 36 (1962) 3489.
- [36] J.H. Ammeter, H.-B. Bürgi, J.C. Thiebault, R. Hoffmann, *J. Am. Chem. Soc.* 100 (1978) 3686.
- [37] C. Mealli, D.M. Proserpio, *J. Chem. Ed.* 67 (1990) 39.
- [38] I.V. Nelson, R.T. Iwamoto, *Anal. Chem.* 35 (1990) 867.